ACS Photonics

Article

pubs.acs.org/journal/apchd5

Optical Magnetism and Fundamental Modes of Nanodiamonds

Daniil A. Shilkin,[†,‡] Maxim R. Shcherbakov,[†] Evgeny V. Lyubin,[†] Konstantin G. Katamadze,[†,§,⊥] Oleg S. Kudryavtsev,[∥] Vadim S. Sedov,[∥] Igor I. Vlasov,[∥,§] and Andrey A. Fedyanin*[,†]

[†]Faculty of Physics, Lomonosov Moscow State University, Moscow 119991, Russia

[‡]Center for Functionalized Magnetic Materials, Immanuel Kant Baltic Federal University, Kaliningrad 236041, Russia

[§]National Research Nuclear University MEPhI, Moscow 115409, Russia

[⊥]Institute of Physics and Technology, Russian Academy of Sciences, Moscow 117218, Russia

[∥]Prokhorov General Physics Institute, Russian Academy of Sciences, Moscow 119991, Russia

Supporting Information

ABSTRACT: The optical properties of color centers in nanodiamonds are widely used in various branches of photonics and interdisciplinary studies. Here, we report on an experimental study of the fundamental eigenmodes of subwavelength diamond nanoparticles. The eigenmodes reveal themselves as scattering resonances, which were measured by single-particle dark-field spectroscopy and calculated both numerically and analytically. The resonances experience a red-shift with increasing particle size, and in the case of an anisotropic particle, they change depending on the polarization of the input light. As an example of an application, the Purcell enhancement of the dipole emission from such nanodiamonds is numerically demonstrated. This study demonstrates a simple way to improve the efficiency of diamond-based sensors and single-photon sources by choosing nanoparticles of optimal size and shape.

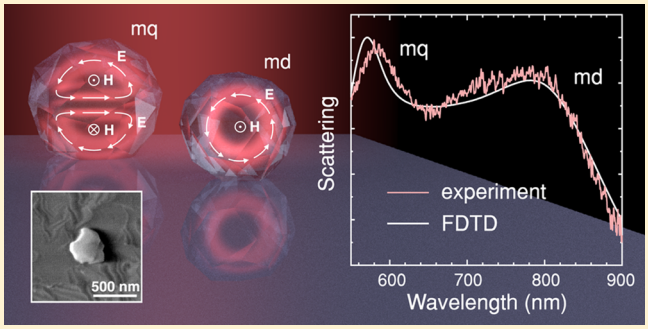

KEYWORDS: *nanodiamonds, Mie resonances, Purcell enhancement, dark-field spectroscopy, chemical vapor deposition*

Nanodiamonds are a novel class of objects with a plethora of applications in various branches of photonics and interdisciplinary studies. They are extensively used as low-toxicity, nonbleaching, luminescent biomarkers,[1−4] precise nanoscale magnetometers,[5−8] and thermometers.[9] Some that contain exactly one center can be used as single-photon sources[10−16] and nodes in quantum computing networks.[17,18] In all of the listed applications, the spectral properties of nanodiamonds should be taken into account. They are especially important in quantum optics, where efficient photon emission into a single optical mode is of paramount importance. Conventionally, this is done by coupling color centers to waveguides[10,11] and resonators;[12−16] however, the intrinsic optical resonances of nanodiamonds themselves are routinely omitted from consideration. Few studies have mentioned the effects of the particle size on the luminescence in submicrometer diamonds,[16,19−22] and there has been no comprehensive study on this problem so far.

High-index nanoparticles possess a set of eigenmodes, including the fundamental magnetic dipole mode. Due to their manifestation in scattering spectra, they are also referred to as Mie resonance modes. Currently, the magnetic dipole mode has been verified in silicon,[23,24] germanium,[25,26] gallium arsenide,[27] and barium titanate perovskite[28] nanoparticles in the visible range and in tellurium[29] microparticles in the mid-infrared. This mode has become the underlying reason for optical magnetism and led to a number of novel devices, such as superdirective scatterers[30−32] and Huygens-type,[33] holographic,[34] beam-deflecting,[35,36] and beam-shaping metasurfaces.[36,37] In addition, it has provided for the enhancement of nonlinearities,[38−40] emission shaping,[41] and Raman response[42] by all-dielectric nanostructures. The high refractive index of diamond allows for the observation of optical magnetism in nanodiamonds, although no evidence of this has been provided so far.

In this article, we demonstrate the fundamental eigenmodes of subwavelength nanodiamonds by scattering spectroscopy performed on single particles with predetermined sizes and shapes. Dark-field scattering spectroscopy reveals pronounced magnetic dipole and quadrupole modes, as verified by calculations performed both analytically and numerically. Further applications of the observed resonances are discussed, and as an example, the Purcell enhancement of dipolar radiation is numerically demonstrated.

Throughout this work, we will limit the consideration of the eigenmodes to magnetic dipole, electric dipole, magnetic quadrupole, and electric quadrupole modes, as they are the lowest-order modes and provide the highest light confinement

Received: January 4, 2017
Published: April 4, 2017

DOI: 10.1021/acsphotonics.7b00007
ACS Photonics 2017, 4, 1153−1158

within a dielectric sphere. The magnetic modes are typically of higher quality factors than the electric ones, and therefore, they are expected to be more apparent in the scattering spectra. In Figure 1a, a schematic representation of the electric and magnetic fields of the lowest-order magnetic Mie resonances in the nanodiamonds is shown. The particles are illuminated by light propagating vertically and polarized in the plane of the schematic. At a certain ratio between the particle size d and the wavelength λ, the electric field on the upper side of the particle is in antiphase with the electric field on the bottom side, which causes circular displacement currents and an enhancement of the magnetic field in the center, leading to the excitation of the magnetic dipole. At the magnetic quadrupole resonance, which is excited at larger d/λ ratios, two magnetic dipoles of opposite phases are efficiently excited. Depending on the size and shape of the particle, its eigenmodes are excited at different wavelengths. In the case of identical shapes, the larger the particle is, the farther to the red the resonances are located. In our experiments, particles of a few hundred nanometers in size that were grown by chemical vapor deposition from detonation seeds on a sapphire substrate were studied; see Supporting Information, Section I, for details of the fabrication procedure. The substrate with the grown diamonds was mapped beforehand so that we could match the images from the microscopes to the measured spectra; see Supporting Information, Figure S2, for the maps. As indicated in the inset of Figure 1b, the shape of the particles is not spherical, but the use of a spherical shape for the calculations gives appropriate results.

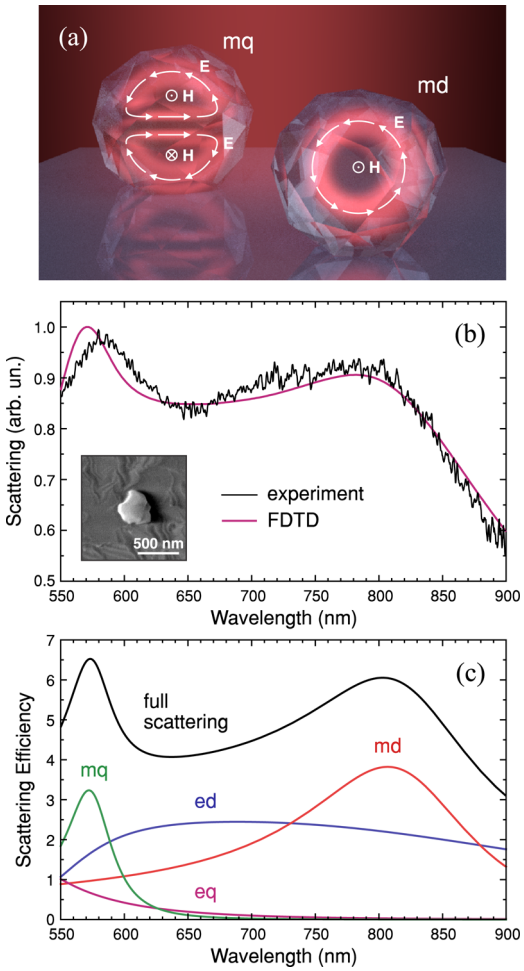

Figure 1. Mie resonances in nanodiamonds. (a) Schematic representation of the fields in nanodiamonds upon excitation of the magnetic dipole (md) and magnetic quadrupole (mq) modes. (b) Unpolarized scattering spectrum from a typical nanodiamond (a scanning electron micrograph is shown in the inset) and FDTD-simulated spectrum of scattering by a sphere with a diameter of 320 nm under the experimental conditions of the collection. (c) Scattering from a free-standing sphere with a diameter of 320 nm calculated by Mie theory.[43] The overall scattering efficiency and the contributions of the electric (e) and magnetic (m) dipole (ed, md) and quadrupole (eq, mq) modes are shown.

In Figure 1b, a scattering spectrum of a typical nanodiamond particle measured by dark-field single-particle spectroscopy is shown, as indicated by the black curve. The illumination light was unpolarized in the measurements; see Supporting Information, Section II, for a description of the setup. A scanning electron micrograph of the particle is shown in the inset. Two peaks are clearly identified in the spectrum, with the resonance at λ = 585 nm being of a larger quality factor than that of the resonance at λ = 800 nm. The results of a finite-difference time-domain (FDTD) simulation that are given in Figure 1b by the purple curve have excellent agreement with the experimental measurement results. In this simulation, a diamond sphere with a diameter of 320 nm that was placed on a sapphire substrate was illuminated by plane-wave radiation, and the far-field scattering was analyzed to simulate the experimental light collection conditions; see Supporting Information, Section V, for details of the calculation.

Scattering spectra for an isolated spherical particle can also be calculated analytically by Mie theory.[43] Figure 1c presents the spectrum of the overall scattering efficiency $Q = C/\pi r^2$, where C is the scattering cross section and r = 160 nm is the radius of the sphere, for a sphere in a vacuum and the contributions of the different Mie modes to the scattering efficiency. In the absence of the substrate, the peaks are more clearly identified, but their positions are not significantly changed. Plotting the contributions of individual Mie coefficients separately shows that the peak at λ = 800 nm is associated with the magnetic dipole resonance, while the peak at λ = 573 nm is due to the magnetic quadrupole resonance.

To observe the size dependence of the resonance positions, diamond nanoparticles with different sizes and shapes were analyzed. Figure 2 presents typical measured scattering spectra of such nanodiamonds. Depending on the dimensions of the particles, one or two peaks can be identified in the spectral region of interest. For the smallest particles, one peak is observed, which we associate with the magnetic dipole resonance. As the particle size increases, the magnetic dipole resonance shifts to the red, and a higher-quality peak appears in the registration range, which is due to the magnetic quadrupole excitation.

Along with their scattering properties, more than 20 nanoparticles were analyzed using scanning electron microscopy. For every particle, the area A and perimeter P were determined based on the images. Then, the effective size $(d = 2\sqrt{A/\pi})$ and circularity $(f = 4\pi A/P^2)$ were calculated. Figure 3 shows the positions of the resonance peaks as a function of the effective particle size. The experimental dependences are shown in Figure 3a. Two groups of points are clearly identified on the plot. We associate one of them with the magnetic dipole resonance (blue circles) and the other with the magnetic quadrupole resonance (purple circles). The

DOI: 10.1021/acsphotonics.7b00007
ACS Photonics 2017, 4, 1153−1158

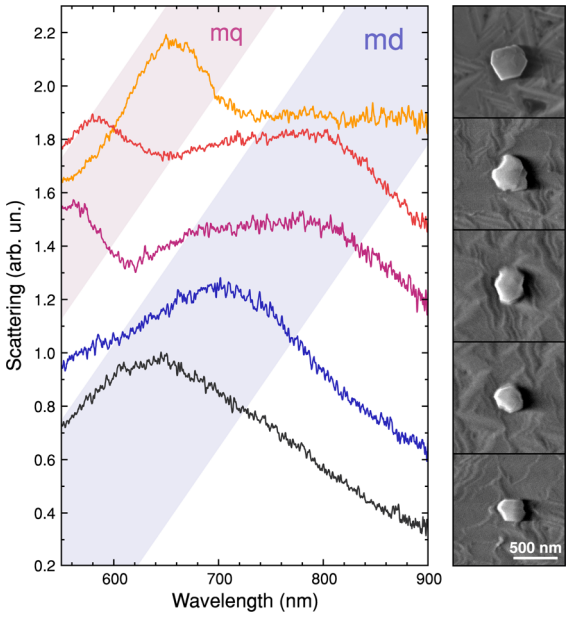

Figure 2. Unpolarized scattering spectra of nanodiamonds with effective diameters of 281 nm (black), 306 nm (blue), 355 nm (purple), 386 nm (red), and 394 nm (yellow) normalized by the maximum value and vertically shifted by the value of 0.3 for better readability. The corresponding scanning electron micrographs are given on the right side of the figure.

dispersion of the data points is partially caused by the variety of the particle shapes available. If one chooses only sphere-like particles ($f > 0.9$, indicated by filled circles on the plot), the dispersion is lower.

The scattering efficiency of a free-standing diamond sphere as a function of the wavelength and the particle size was calculated using Mie theory[43] and is shown in Figure 3b. The same dependence obtained by the FDTD simulations for a diamond sphere on a sapphire substrate under the experimental collection conditions is given in Figure 3c. The resonances are not as clear without the substrate, but their positions do not change significantly. The positions of the resonances obtained from the FDTD simulations are plotted in Figure 3a by dashed lines. The experimentally observed shift of the resonances is in good agreement with the calculation, but the experimentally obtained resonances are shifted to the blue side of the spectrum compared to the calculation results. The resonances of the sphere-like particles are closer to the calculation results.

The shapes of nanoparticles greatly affect their optical properties, including those that depend on the polarization of incoming light. Anisotropy is a useful degree of freedom when tailoring the optical properties of Mie-resonant nanodiamonds. The scattering by an anisotropic nanodiamond at approximately 700 nm is shown in Figure 4a as a function of the input polarization. The change in scattering at this wavelength is approximately 30% at a particle circularity of 0.84. Figure 4b presents scattering spectra with the illumination polarized along the perpendicular directions. FDTD-simulated scattering for a prolate spheroid with a long axis of 400 nm and a short axis of 330 nm is shown in Figure 4c. Although the spheroid approximation is the simplest, the calculated spectra are in good qualitative agreement with the experimental data.

The resonances studied in this work can reveal themselves in a variety of processes in single nanodiamonds. For instance, Mie resonances were mentioned as a possible explanation of

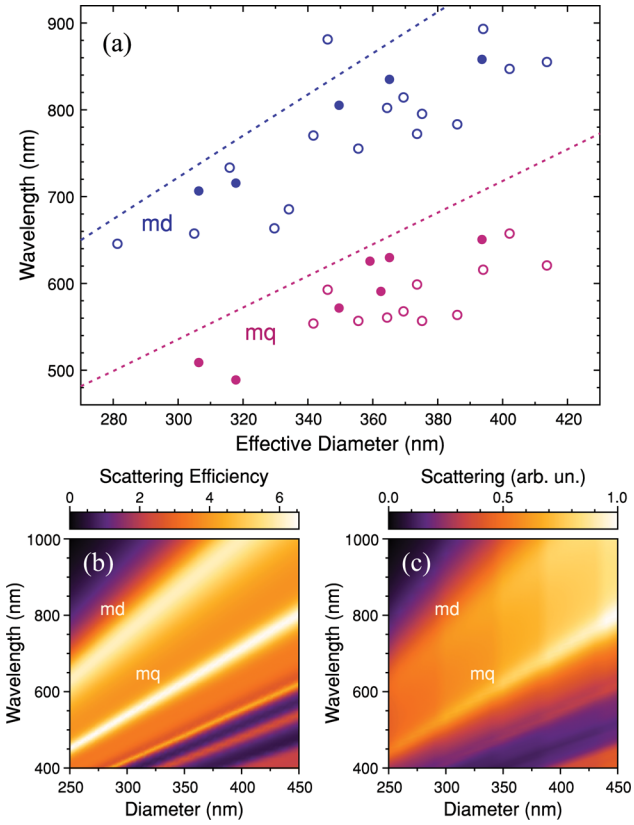

Figure 3. Positions of the Mie resonances depending on the size of the diamonds. (a) Experimental dependences of the resonance peak positions in the unpolarized scattering spectra. The points for particles with circularity $f > 0.9$ are shown as filled circles. The lines show the resonance peak positions obtained by FDTD calculations for spherical shapes under the experimental collection conditions. (b) Scattering by a free-standing sphere calculated by Mie theory.[43] (c) FDTD-calculated scattering by a sphere on a sapphire substrate under the experimental collection conditions.

the experimentally observed large dispersion in the lifetime of the excited state of chromium-related centers in nanodiamonds of various sizes.[21] The reduction—or increase—in the lifetime of the excited state in a resonator compared to that observed in a homogeneous environment is called the Purcell effect. This effect has been theoretically shown to occur during the excitation of Mie resonances in a high-permittivity sphere[44] and, consequently, may be observed in nanodiamonds, as numerically confirmed for a number of geometries.[20,45,46] The Purcell factor calculated for an electric dipole located inside a subwavelength diamond sphere has been previously shown to depend non-monotonically on the particle size.[20−22] As we show below, this dependence can be interpreted by coupling with the particle eigenmodes, and new features can be found in the dependence on the position of the dipole inside the sphere.

The Purcell effect in a diamond nanoparticle was quantified using FDTD simulations of the emission of an oscillating electric dipole located at different positions inside a free-standing diamond sphere with a diameter of 320 nm. The Purcell factor was determined by calculating the emission energy of the dipole and dividing it by that emitted by the dipole in bulk diamond. The result is shown in Figure 5a,b as a function of the dipole position and the wavelength of radiation in a vacuum corresponding to the dipole oscillating frequency. The spectral dependence of the Purcell enhancement can be

DOI: 10.1021/acsphotonics.7b00007
ACS Photonics 2017, 4, 1153−1158

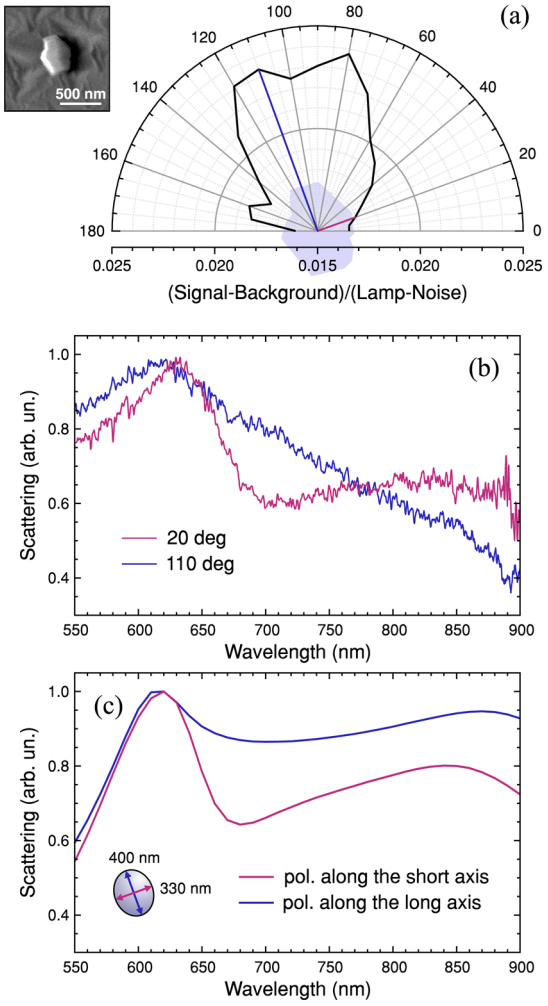

Figure 4. (a) Scattering by an anisotropic diamond nanoparticle with an effective diameter of 394 nm and a circularity of 0.84. The scattering at the wavelength of 700 ± 5 nm is shown as a function of the illumination polarization. A scanning electron micrograph of the particle is shown in the inset. The particle orientation is shown in the background. (b) Scattering spectra for the anisotropic nanodiamond for two perpendicular polarizations. (c) FDTD-simulated spectra of scattering by a prolate spheroid with a long axis of 400 nm and a short axis of 330 nm on a sapphire substrate under the experimental collection conditions.

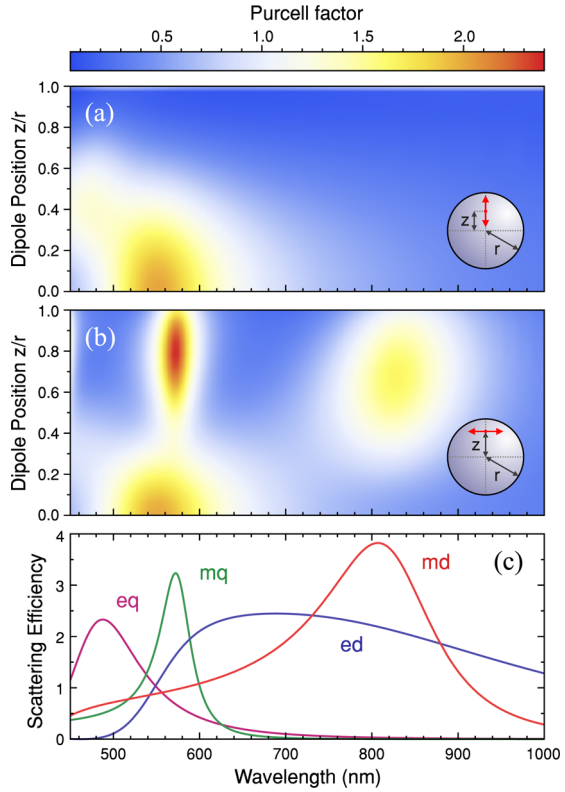

Figure 5. Purcell effect in a free-standing diamond sphere with a diameter of $2r$ = 320 nm. (a, b) Dependence of the Purcell factor on the wavelength in a vacuum and the distance z between the center of the sphere and the dipole. The dipole is oriented (a) along the radius; (b) tangentially. The plots have the same color scale. (c) Efficiency of the scattering by the sphere contributed by the electric (e) and magnetic (m) dipoles (ed, md) and quadrupoles (eq, mq).

interpreted by comparison with the scattering spectra of the fundamental modes. The contributions of the four fundamental modes to scattering from the same sphere are shown in Figure 5c. When a radiating dipole is located in the center, the Purcell enhancement takes place only on the blue side of the electric dipole scattering resonance. When the dipole is significantly displaced from the center, the Purcell factor strongly depends on the dipole orientation. In the case of the radial direction represented by Figure 5a, an enhancement takes place around the wavelength corresponding to the electric quadrupole resonance, whereas the magnetic modes have no effect on the dipole radiation because of the symmetry. In the case of the tangential direction (Figure 5b), the Purcell factor is strongly enhanced at the wavelengths corresponding to the magnetic dipole and quadrupole resonances.

The maximum Purcell factor observed for the nanoparticles under consideration is equal to 2.4; this value is significantly larger than the value of 0.06 reported for a diamond sphere in the Rayleigh limit.[20,47,48] The change of the shape to spheroids leads to the shift of the resonances, but the values of the Purcell enhancement do not change dramatically; see Supporting Information, Section VI, for details. The almost two-order enhancement of the Purcell factor, compared to a nonresonant nanoparticle, clearly demonstrates the importance of taking Mie resonances into account when considering the optical properties of single nanodiamonds. In contrast to smaller nanodiamonds,[49,50] Mie-resonant particles provide nonblinking luminescence at the same time, being much more compact than other resonators.[12−16,48] At the wavelength of the magnetic quadrupole, the Purcell enhancement for the tangentially oriented dipole occurs for any position of the dipole within the nanodiamond. As shown in the previous sections, the resonances can be easily adjusted by changing the size of the particle to obtain the optimum value of the Purcell factor for a given wavelength of a color center used.

In addition to the change in the emission rate, resonators also affect the directivity of the dipole emission and, with an appropriate design, can be used as directional antennas.[31,51] With methods that improve the collection efficiency,[20,46,52] Mie-resonant nanoparticles shown here can become a powerful tool in diamond photonics.

In conclusion, we have experimentally demonstrated the fundamental eigenmodes of subwavelength nanodiamonds. We have used chemical vapor deposition of large nanodiamonds from detonation seeds and subsequent scattering spectroscopy to reveal the eigenmodes of single nanodiamonds. We have

DOI: 10.1021/acsphotonics.7b00007
ACS Photonics 2017, 4, 1153−1158

shown that the magnetic dipole and quadrupole modes are the most dominant in the visible range. The results have been verified by calculations performed both analytically and numerically. The magnetic dipole and magnetic quadrupole modes of single nanodiamonds have been shown to shift with increasing particle size; in the case of an anisotropic particle, the modes are modified by varying the input light polarization orientation. The importance of taking diamond eigenmodes into account has been demonstrated by the almost two-order enhancement of the Purcell factor in the case of magnetic quadrupole resonance of a subwavelength nanoparticle compared with that of a nonresonant nanoparticle.

■ ASSOCIATED CONTENT

Supporting Information

The Supporting Information is available free of charge on the ACS Publications website at DOI: 10.1021/acsphotonics.7b00007.

Detailed descriptions of the fabrication of the nanodiamonds, the experimental setup, the characterization of the nanodiamonds, the processing of the scattering spectra, the numerical calculations, and the analysis of the Purcell enhancement in spheroidal particles (PDF)

■ AUTHOR INFORMATION

Corresponding Author

*E-mail: fedyanin@nanolab.phys.msu.ru.

ORCID

Andrey A. Fedyanin: 0000-0003-4708-6895

Notes

The authors declare no competing financial interest.

■ ACKNOWLEDGMENTS

The authors acknowledge stimulating discussions with Alexander Shorokhov, Boris Luk'yanchuk, and Yuri Kivshar. This work was partially supported by the Russian Ministry of Education and Science (#14.W03.31.0008), the Russian Foundation for Basic Research (#16-29-11811, spectroscopy experiments), the Grant of the President of the Russian Federation (#MK-5860.2016.2, calculations), and the Russian Science Foundation (#14-12-01329, synthesis and characterization of the nanodiamonds).

■ REFERENCES

(1) Yu, S.-J.; Kang, M.-W.; Chang, H.-C.; Chen, K.-M.; Yu, Y.-C. Bright fluorescent nanodiamonds: no photobleaching and low cytotoxicity. *J. Am. Chem. Soc.* **2005**, *127*, 17604−17605.

(2) Fu, C.-C.; Lee, H.-Y.; Chen, K.; Lim, T.-S.; Wu, H.-Y.; Lin, P.-K.; Wei, P.-K.; Tsao, P.-H.; Chang, H.-C.; Fann, W. Characterization and application of single fluorescent nanodiamonds as cellular biomarkers. *Proc. Natl. Acad. Sci. U. S. A.* **2007**, *104*, 727−732.

(3) Faklaris, O.; Joshi, V.; Irinopoulou, T.; Tauc, P.; Sennour, M.; Girard, H.; Gesset, C.; Arnault, J.-C.; Thorel, A.; Boudou, J.-P.; Curmi, P. A.; Treussart, F. Photoluminescent diamond nanoparticles for cell labeling: study of the uptake mechanism in mammalian cells. *ACS Nano* **2009**, *3*, 3955−3962.

(4) Vaijayanthimala, V.; Lee, D. K.; Kim, S. V.; Yen, A.; Tsai, N.; Ho, D.; Chang, H.-C.; Shenderova, O. Nanodiamond-mediated drug delivery and imaging: challenges and opportunities. *Expert Opin. Drug Delivery* **2015**, *12*, 735−749.

(5) Balasubramanian, G.; Chan, I. Y.; Kolesov, R.; Al-Hmoud, M.; Tisler, J.; Shin, C.; Kim, C.; Wojcik, A.; Hemmer, P. R.; Krueger, A.; Hanke, T.; Leitenstorfer, A.; Bratschitsch, R.; Jelezko, F.; Wrachtrup, J. Nanoscale imaging magnetometry with diamond spins under ambient conditions. *Nature* **2008**, *455*, 648−651.

(6) Schoenfeld, R. S.; Harneit, W. Real time magnetic field sensing and imaging using a single spin in diamond. *Phys. Rev. Lett.* **2011**, *106*, 030802.

(7) Schirhagl, R.; Chang, K.; Loretz, M.; Degen, C. L. Nitrogen-vacancy centers in diamond: nanoscale sensors for physics and biology. *Annu. Rev. Phys. Chem.* **2014**, *65*, 83−105.

(8) Fedotov, I. V.; Blakley, S. M.; Serebryannikov, E. E.; Hemmer, P.; Scully, M. O.; Zheltikov, A. M. High-resolution magnetic field imaging with a nitrogen-vacancy diamond sensor integrated with a photonic-crystal fiber. *Opt. Lett.* **2016**, *41*, 472−475.

(9) Tzeng, Y.-K.; Tsai, P.-C.; Liu, H.-Y.; Chen, O. Y.; Hsu, H.; Yee, F.-G.; Chang, M.-S.; Chang, H.-C. Time-resolved luminescence nanothermometry with nitrogen-vacancy centers in nanodiamonds. *Nano Lett.* **2015**, *15*, 3945−3952.

(10) Schröder, T.; Schell, A. W.; Kewes, G.; Aichele, T.; Benson, O. Fiber-integrated diamond-based single photon source. *Nano Lett.* **2011**, *11*, 198−202.

(11) Liebermeister, L.; Petersen, F.; Münchow, A. v.; Burchardt, D.; Hermelbracht, J.; Tashima, T.; Schell, A. W.; Benson, O.; Meinhardt, T.; Krueger, A.; Stiebeiner, A.; Rauschenbeutel, A.; Weinfurter, H.; Weber, M. Tapered fiber coupling of single photons emitted by a deterministically positioned single nitrogen vacancy center. *Appl. Phys. Lett.* **2014**, *104*, 031101.

(12) Wolters, J.; Schell, A. W.; Kewes, G.; Nüsse, N.; Schoengen, M.; Döscher, H.; Hannappel, T.; Löchel, B.; Barth, M.; Benson, O. Enhancement of the zero phonon line emission from a single nitrogen vacancy center in a nanodiamond via coupling to a photonic crystal cavity. *Appl. Phys. Lett.* **2010**, *97*, 141108.

(13) De Leon, N. P.; Shields, B. J.; Yu, C. L.; Englund, D. E.; Akimov, A. V.; Lukin, M. D.; Park, H. Tailoring light-matter interaction with a nanoscale plasmon resonator. *Phys. Rev. Lett.* **2012**, *108*, 226803.

(14) Schell, A. W.; Kaschke, J.; Fischer, J.; Henze, R.; Wolters, J.; Wegener, M.; Benson, O. Three-dimensional quantum photonic elements based on single nitrogen vacancy-centres in laser-written microstructures. *Sci. Rep.* **2013**, *3*, 1577.

(15) Albrecht, R.; Bommer, A.; Pauly, C.; Mücklich, F.; Schell, A. W.; Engel, P.; Schröder, T.; Benson, O.; Reichel, J.; Becher, C. Narrow-band single photon emission at room temperature based on a single nitrogen-vacancy center coupled to an all-fiber-cavity. *Appl. Phys. Lett.* **2014**, *105*, 073113.

(16) Kaupp, H.; Hümmer, T.; Mader, M.; Schlederer, B.; Benedikter, J.; Haeusser, P.; Chang, H.-C.; Fedder, H.; Hänsch, T. W.; Hunger, D. Purcell-enhanced single-photon emission from nitrogen-vacancy centers coupled to a tunable microcavity. *Phys. Rev. Appl.* **2016**, *6*, 54010.

(17) Johnson, S.; Dolan, P. R.; Grange, T.; Trichet, A. A. P.; Hornecker, G.; Chen, Y.-C.; Weng, L.; Hughes, G. M.; Watt, A. A. R.; Auffèves, A.; Smith, J. M. Tunable cavity coupling of the zero phonon line of a nitrogen-vacancy defect in diamond. *New J. Phys.* **2015**, *17*, 122003.

(18) Greentree, A. D. Nanodiamonds in Fabry-Perot cavities: a route to scalable quantum computing. *New J. Phys.* **2016**, *18*, 021002.

(19) Chung, P.-H.; Perevedentseva, E.; Cheng, C.-L. The particle size-dependent photoluminescence of nanodiamonds. *Surf. Sci.* **2007**, *601*, 3866−3870.

(20) Greffet, J.-J.; Hugonin, J.-P.; Besbes, M.; Lai, N. D.; Treussart, F.; Roch, J.-F. Diamond particles as nanoantennas for nitrogen-vacancy color centers. *arXiv*, 2011, 1107.0502.

(21) Castelletto, S.; Boretti, A. Radiative and nonradiative decay rates in chromium-related centers in nanodiamonds. *Opt. Lett.* **2011**, *36*, 4224−4226.

(22) Inam, F. A.; Steel, M. J.; Castelletto, S. Effects of the hosting nano-environment modifications on NV centres fluorescence emission. *Diamond Relat. Mater.* **2014**, *45*, 64−69.

(23) Kuznetsov, A. I.; Miroshnichenko, A. E.; Fu, Y. H.; Zhang, J.; Luk'yanchuk, B. Magnetic light. *Sci. Rep.* **2012**, *2*, 492.

DOI: 10.1021/acsphotonics.7b00007
ACS Photonics 2017, 4, 1153−1158

(24) Evlyukhin, A. B.; Novikov, S. M.; Zywietz, U.; Eriksen, R. L.; Reinhardt, C.; Bozhevolnyi, S. I.; Chichkov, B. N. Demonstration of magnetic dipole resonances of dielectric nanospheres in the visible region. *Nano Lett.* **2012**, *12*, 3749−3755.
(25) Gómez-Medina, R.; García-Cámara, B.; Suárez-Lacalle, I.; González, F.; Moreno, F.; Nieto-Vesperinas, M.; Sáenz, J. J. Electric and magnetic dipolar response of germanium nanospheres: Interference effects, scattering anisotropy and optical forces. *J. Nanophotonics* **2011**, *5*, 053512−053519.
(26) Lewi, T.; Iyer, P. P.; Butakov, N. A.; Mikhailovsky, A. A.; Schuller, J. A. Widely tunable infrared antennas using free carrier refraction. *Nano Lett.* **2015**, *15*, 8188−8193.
(27) Liu, S.; Keeler, G. A.; Reno, J. L.; Sinclair, M. B.; Brener, I. III−V semiconductor nanoresonators—a new strategy for passive, active, and nonlinear all-dielectric metamaterials. *Adv. Opt. Mater.* **2016**, *4*, 1457−1462.
(28) Timpu, F.; Sergeyev, A.; Hendricks, N. R.; Grange, R. Second-harmonic enhancement with Mie resonances in perovskite nanoparticles. *ACS Photonics* **2017**, *4*, 76−84.
(29) Ginn, J. C.; Brener, I.; Peters, D. W.; Wendt, J. R.; Stevens, J. O.; Hines, P. F.; Basilio, L. I.; Warne, L. K.; Ihlefeld, J. F.; Clem, P. G.; Sinclair, M. B. Realizing optical magnetism from dielectric metamaterials. *Phys. Rev. Lett.* **2012**, *108*, 097402.
(30) Fu, Y. H.; Kuznetsov, A. I.; Miroshnichenko, A. E.; Yu, Y. F.; Luk'yanchuk, B. Directional visible light scattering by silicon nanoparticles. *Nat. Commun.* **2013**, *4*, 1527.
(31) Staude, I.; Miroshnichenko, A. E.; Decker, M.; Fofang, N. T.; Liu, S.; Gonzales, E.; Dominguez, J.; Luk, T. S.; Neshev, D. N.; Brener, I.; Kivshar, Y. Tailoring directional scattering through magnetic and electric resonances in subwavelength silicon nanodisks. *ACS Nano* **2013**, *7*, 7824−7832.
(32) Luk'yanchuk, B. S.; Voshchinnikov, N. V.; Paniagua-Domínguez, R.; Kuznetsov, A. I. Optimum forward light scattering by spherical and spheroidal dielectric nanoparticles with high refractive index. *ACS Photonics* **2015**, *2*, 993−999.
(33) Decker, M.; Staude, I.; Falkner, M.; Dominguez, J.; Neshev, D. N.; Brener, I.; Pertsch, T.; Kivshar, Y. S. High-efficiency dielectric Huygens' surfaces. *Adv. Opt. Mater.* **2015**, *3*, 813−820.
(34) Chong, K. E.; Wang, L.; Staude, I.; James, A. R.; Dominguez, J.; Liu, S.; Subramania, G. S.; Decker, M.; Neshev, D. N.; Brener, I.; Kivshar, Y. S. Efficient polarization insensitive complex wavefront control using Huygens' metasurfaces based on dielectric resonant meta-atoms. *ACS Photonics* **2016**, *3*, 514−519.
(35) Yu, Y. F.; Zhu, A. Y.; Paniagua-Domínguez, R.; Fu, Y. H.; Luk'yanchuk, B.; Kuznetsov, A. I. High-transmission dielectric metasurface with 2 π phase control at visible wavelengths. *Laser Photon. Rev.* **2015**, *9*, 412−418.
(36) Shalaev, M. I.; Sun, J.; Tsukernik, A.; Pandey, A.; Nikolskiy, K.; Litchinitser, N. M. High-efficiency all-dielectric metasurfaces for ultracompact beam manipulation in transmission mode. *Nano Lett.* **2015**, *15*, 6261−6266.
(37) Chong, K. E.; Staude, I.; James, A.; Dominguez, J.; Liu, S.; Campione, S.; Subramania, G. S.; Luk, T. S.; Decker, M.; Neshev, D. N.; Brener, I.; Kivshar, Y. S. Polarization-independent silicon metadevices for efficient optical wavefront control. *Nano Lett.* **2015**, *15*, 5369−5374.
(38) Shcherbakov, M. R.; Neshev, D. N.; Hopkins, B.; Shorokhov, A. S.; Staude, I.; Melik-Gaykazyan, E. V.; Decker, M.; Ezhov, A. A.; Miroshnichenko, A. E.; Brener, I.; Fedyanin, A. A.; Kivshar, Y. S. Enhanced third-harmonic generation in silicon nanoparticles driven by magnetic response. *Nano Lett.* **2014**, *14*, 6488−6492.
(39) Shcherbakov, M. R.; Shorokhov, A. S.; Neshev, D. N.; Hopkins, B.; Staude, I.; Melik-Gaykazyan, E. V.; Ezhov, A. A.; Miroshnichenko, A. E.; Brener, I.; Fedyanin, A. A.; Kivshar, Y. S. Nonlinear interference and tailorable third-harmonic generation from dielectric oligomers. *ACS Photonics* **2015**, *2*, 578−582.
(40) Shorokhov, A. S.; Melik-Gaykazyan, E. V.; Smirnova, D. A.; Hopkins, B.; Chong, K. E.; Choi, D.-Y.; Shcherbakov, M. R.; Miroshnichenko, A. E.; Neshev, D. N.; Fedyanin, A. A.; Kivshar, Y. S. Multifold enhancement of third-harmonic generation in dielectric nanoparticles driven by magnetic Fano resonances. *Nano Lett.* **2016**, *16*, 4857−4861.
(41) Staude, I.; Khardikov, V. V.; Fofang, N. T.; Liu, S.; Decker, M.; Neshev, D. N.; Luk, T. S.; Brener, I.; Kivshar, Y. S. Shaping photoluminescence spectra with magnetoelectric resonances in all-dielectric nanoparticles. *ACS Photonics* **2015**, *2*, 172−177.
(42) Caldarola, M.; Albella, P.; Cortés, E.; Rahmani, M.; Roschuk, T.; Grinblat, G.; Oulton, R. F.; Bragas, A. V.; Maier, S. A. Non-plasmonic nanoantennas for surface enhanced spectroscopies with ultra-low heat conversion. *Nat. Commun.* **2015**, *6*, 7915.
(43) Bohren, C. F.; Huffman, D. R. *Absorption and Scattering of Light by Small Particles*; John Wiley & Sons: New York, 1998.
(44) Zambrana-Puyalto, X.; Bonod, N. Purcell factor of spherical Mie resonators. *Phys. Rev. B: Condens. Matter Mater. Phys.* **2015**, *91*, 195422.
(45) Shugayev, R.; Bermel, P. Core-shell Mie resonant structures for quantum computing applications. *Appl. Phys. Lett.* **2016**, *109*, 221102.
(46) Hong, H.-G.; Lee, S.-B.; Heo, M.-S.; Park, S. E.; Kwon, T. Y. Mie resonance-enhanced pumping and detection efficiency for shallow nitrogen-vacancy centers in diamond. *Opt. Express* **2016**, *24*, 28815−28828.
(47) Inam, F. A.; Grogan, M. D. W.; Rollings, M.; Gaebel, T.; Say, J. M.; Bradac, C.; Birks, T. A.; Wadsworth, W. J.; Castelletto, S.; Rabeau, J. R.; Steel, M. J. Emission and nonradiative decay of nanodiamond NV centers in a low refractive index environment. *ACS Nano* **2013**, *7*, 3833−3843.
(48) Riedrich-Möller, J.; Arend, C.; Pauly, C.; Mücklich, F.; Fischer, M.; Gsell, S.; Schreck, M.; Becher, C. Deterministic coupling of a single silicon-vacancy color center to a photonic crystal cavity in diamond. *Nano Lett.* **2014**, *14*, 5281−5287.
(49) Vlasov, I. I.; Shiryaev, A. A.; Rendler, T.; Steinert, S.; Lee, S.-Y.; Antonov, D.; Voros, M.; Jelezko, F.; Fisenko, A. V.; Semjonova, L. F.; Biskupek, J.; Kaiser, U.; Lebedev, O. I.; Sildos, I.; Hemmer, P. R.; Konov, V. I.; Gali, A.; Wrachtrup, J. Molecular-sized fluorescent nanodiamonds. *Nat. Nanotechnol.* **2014**, *9*, 54−58.
(50) Shershulin, V. A.; Sedov, V. S.; Ermakova, A.; Jantzen, U.; Rogers, L.; Huhlina, A. A.; Teverovskaya, E. G.; Ralchenko, V. G.; Jelezko, F.; Vlasov, I. I. Size-dependent luminescence of color centers in composite nanodiamonds. *Phys. Status Solidi A* **2015**, *212*, 2600−2605.
(51) Krasnok, A. E.; Simovski, C. R.; Belov, P. A.; Kivshar, Y. S. Superdirective dielectric nanoantennas. *Nanoscale* **2014**, *6*, 7354−7361.
(52) Krasnok, A. E.; Maloshtan, A.; Chigrin, D. N.; Kivshar, Y. S.; Belov, P. A. Enhanced emission extraction and selective excitation of NV centers with all−dielectric nanoantennas. *Laser Photon. Rev.* **2015**, *9*, 385−391.

DOI: 10.1021/acsphotonics.7b00007
ACS Photonics 2017, 4, 1153−1158